

Supporting Information for

**High-Efficiency SrTiO₃/TiO₂ Hetero-Photoanode for Visible-Light
Water Splitting by Charge Transport Design and Optical Absorption
Management**

Xiang Cheng,^{a,b} Yajun Zhang,^a Hongyan Hu,^{*a} Mingdong Shang^a and Yingpu Bi^{*a}

- a. State Key Laboratory for Oxo Synthesis & Selective Oxidation, and National Engineering Research Center for Fine Petrochemical Intermediates, Lanzhou Institute of Chemical Physics, CAS, Lanzhou 730000, China. *E-mail: yingpubi@licp.cas.cn; huhongyan@licp.cas.cn
- b. University of Chinese Academy of sciences, Beijing 100049, China.

1. Experimental Section

1.1 Chemical reagents and characterization

Titanium foils (0.2 mm, >99.9%) purchased from Baoji Titanium Industry Co., Ltd were used to prepare TiO₂ nanotube arrays (TiO₂ NTs). Ethylene glycol, acetone, sodium hydroxide, hydrofluoric acid, ammonium fluoride, ethanol, nitric acid, Al powder, and sodium hydroxide were purchased from Sinopharm Chemical Reagent Co., Ltd. Strontium hydroxide octahydrate (Sr(OH)₂·8H₂O) was obtained from Alfa Aesar. All the chemicals were of analytical grade and used as received without any further purification, unless otherwise stated. Deionized water (18.25 MΩ, molecular) was used in all experiment steps.

The morphology and size of photoelectrode materials were characterized by field-emission scanning electron microscope (JSM-6701F, JEOL) operated at an accelerating voltage of 5 kV. X-ray diffraction (PANalytical X'Pert PRO) using graphite monochromized Cu K_α radiation (40 kV) was applied for measuring crystal structure of the as-prepared photoanodes. The XRD patterns were recorded from 20° to 80° with a scanning rate of 0.067°/s. UV-visible diffusion reflectance spectra was measured on a UV-2550 (Shimadzu) spectrometer by using BaSO₄ as the reference. X-ray photoelectron spectroscopy (XPS, Kratos Axis Ultra DLD) was performed by using the photoelectron spectrometer (ESCALAB 250xi) with X-ray monochromatisation as the excitation source to analyze elemental composition. Hydrogen gas was detected by a gas chromatograph (GC-7900, Techcomp).

1.2 Preparation of TiO₂, Cr-TiO₂, SrTiO₃, Cr-SrTiO₃ nanotube arrays and Cr-SrTiO₃/Cr-TiO₂ heterostructured nanotube arrays.

First of all, titanium foils were cut into 1 x 3 cm strips. Subsequently, these strips were degreased ultrasonically in turn in acetone, ethanol, and deionized water for about 30 min, and then polished in a 1:1:2 mixture of hydrofluoric acid, nitric acid and deionized water. The TiO₂ NTs were prepared by a two-step electrochemical anodization process with the Ti foil as an anode and a Pt mesh as a cathode. After the Ti foil was immersed in a mixed ethylene glycol solution of ammonium fluoride (0.3 wt %) and deionized water (3 wt %), Ti foil was subjected to a constant 60 V anodic potential for 1h in a two-electrode electrochemical cell connected to a DC power supply. Subsequently, the TiO₂ NTs were removed by violently ultrasound treatment. The same Ti foil underwent the second anodization at 60 V for 30 min. Finally, the prepared TiO₂ NTs were thoroughly cleaned with DI water and dried in N₂ gas. The strip was immersed into the solution

(2.5 mmol L⁻¹ Cr (NO₃)₃·9H₂O) for 24 h. The resulting amorphous TiO₂ NTs and undoped TiO₂ NTs were annealed at 450 °C for 2h with heating and cooling rates of 3 °C min⁻¹ in the atmosphere to crystallize the tube walls.

The Cr-doped TiO₂ NTs obtained in the above step were used as both substrate and reactant for the fabrication of heterostructured Cr-SrTiO₃/Cr-TiO₂ nanotube arrays. In a typical synthesis, 0.025 g Sr(OH)₂·8H₂O, 5 g NaOH and 0.002 g Cr(NO₃)₃·9H₂O were dissolved in 40 ml deionized water as the precursor solution, constantly stirring the solution until completely dissolved. Then, the solution and TiO₂ strip were transferred Teflon-lined stainless steel autoclave. The hydrothermal reaction was carried out at 150 °C in an electric oven for 45 min. After the autoclave was rapidly cooled to room temperature, the sample was taken out and rinsed extensively with deionized water, and then dried at 60 °C for 1 h. The synthesis method of Cr-SrTiO₃ was similar to that of Cr-SrTiO₃/Cr-TiO₂ heterostructures, except that the hydrothermal reaction was carried out at 180 °C for 60 h.¹

1.3 Preparation of Cr-SrTiO_{3-x}/Cr-TiO_{2-x} heterostructures and Cr-TiO_{2-x}, Cr-SrTiO_{3-x} nanotube arrays.

A certain amount of Al powder and heterostructured Cr-SrTiO₃/Cr-TiO₂ nanotube arrays obtained in the above step were separately placed in an evacuated two-zone furnace of 800°C (molten Al) and 450 °C (Cr-SrTiO₃/Cr-TiO₂) for 6 h in a 5×10⁻⁴ Pa pressure. The synthetic approach of Cr-TiO_{2-x} (The Al-reduced Cr-TiO₂, Cr-SrTiO₃ and Cr-SrTiO₃/Cr-TiO₂ samples are denoted as Cr-TiO_{2-x}, Cr-SrTiO_{3-x} and Cr-SrTiO_{3-x}/Cr-TiO_{2-x}, respectively) and Cr-SrTiO_{3-x} was analogous to that of Cr-SrTiO_{3-x}/Cr-TiO_{2-x} heterostructures, except that the 450 °C-zone was corresponding to Cr-TiO₂ and Cr-SrTiO₃.

1.4 Photoconversion and photoelectrochemical hydrogen production.

Photoelectrochemical experiments were carried out on an electrochemical workstation (CHI 660D). The electrochemical system consists of three electrodes with platinum sheet (20×20 mm) as a counter electrode, a saturated calomel electrode (SCE) as the reference electrode, and the heterostructure nanotube arrays as the working electrode, respectively.

The transformation formula is performed using the equation below:

$$E_{\text{RHE}} = E_{\text{SCE (reference)}} + E_{\text{SCE}} + 0.0591 \times \text{pH}$$

Where the $E_{\text{SCE (reference)}} = 0.024\text{V}$ at 25 °C and the pH represent the acidity-basicity value of the

electrolyte. In addition, the 300 W xenon arc lamp equipped with a 420 nm cutoff filter (HSX-F300, Beijing NBeT Technology Co., Ltd) calibrated to 200 mWcm^{-2} , which was measured with a radiometer (CEL-NP2000, Beijing Au-light Co., Ltd), served as light source.

The photocurrent response under monochromatic light was measured by using a 300 W Xe lamp and a monochromator (71SWS, Beijing 7-Star Optical Instruments Co., Ltd) at 0.6 V (vs SCE). EIS measurements were performed by applying 0.6 V (vs SCE) at a frequency range of 1×10^5 Hz to 0.01 Hz with amplitude of 10 mV in the light. The measured spectra were fitted with Z-view. The Mott-Schottky curves were obtained under dark conditions at a frequency of 5 kHz, amplitude ± 10 mV. All experiments were carried out under ambient conditions.

Photoelectrochemical H_2 evolution was investigated in a photoelectrochemical cell, in which the photoanode and the counter electrode were separated by an Amberplex membrane. NaOH (1 mol L^{-1}) was utilized as electrolyte, and all as-prepare electrodes was used as photoanode. A saturated calomel electrode was used as reference electrode. Pt sheet was used as photocathode, respectively.

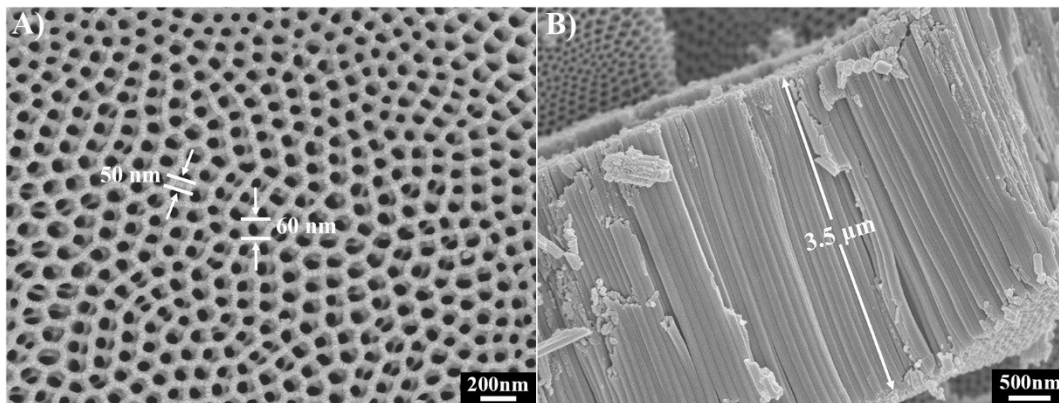


Fig. S1 SEM images of as-prepared TiO_2 nanotube arrays: (A) Top-view and (B) side-view.

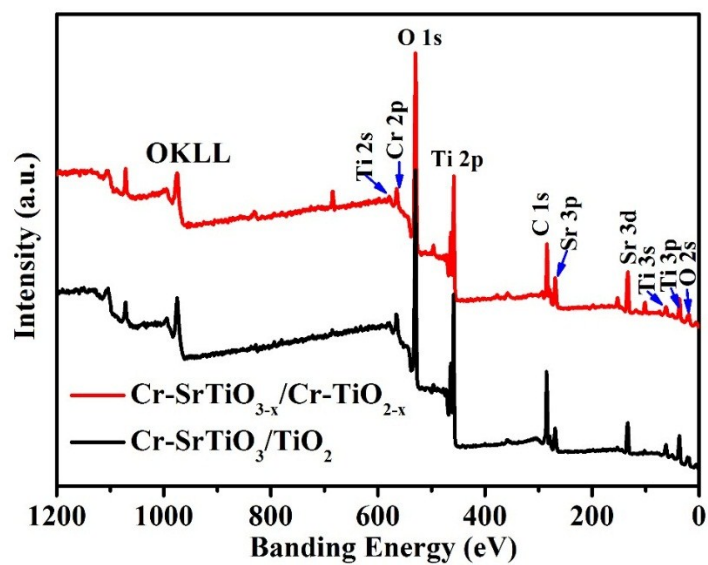


Fig. S2 Full-scan XPS spectrum of $\text{Cr-SrTiO}_3/\text{TiO}_2$ and $\text{Cr-SrTiO}_{3-x}/\text{Cr-TiO}_{2-x}$ heterostructured nanotube arrays after hydrothermal reaction for 45 min.

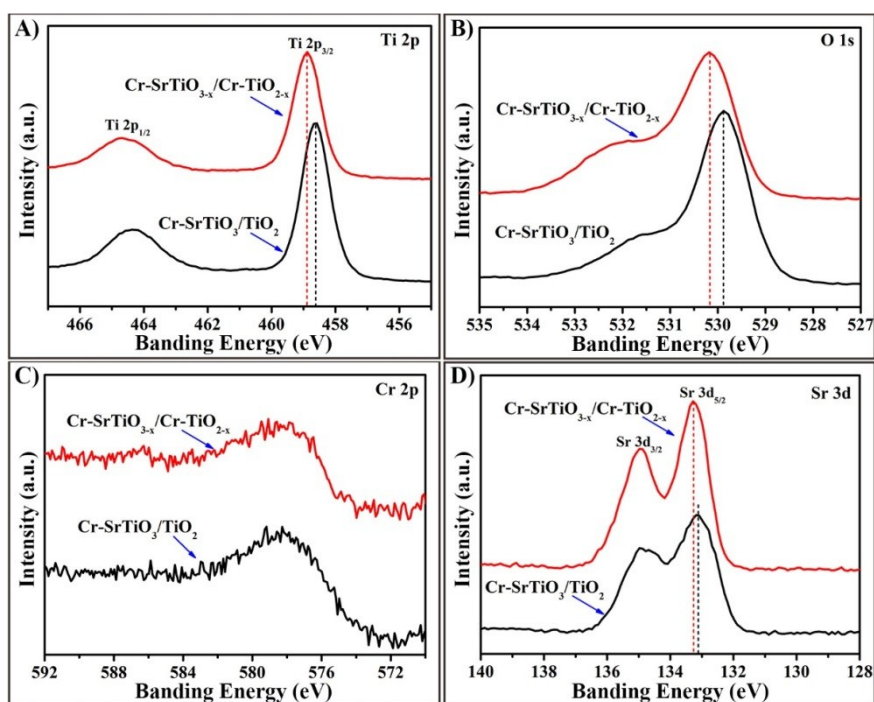


Fig. S3 High-resolution A) Ti 2p, B) O 1s, C) Cr 2p and D) Sr 3d XPS spectra of the Cr-SrTiO_{3-x}/Cr-TiO_{2-x} and Cr-SrTiO_{3-x}/Cr-TiO_{2-x} heterostructured nanotube arrays after hydrothermal reaction for 45 min.

Results and discussions

To further clarify the chemical states and composition of as-prepared Cr-SrTiO_{3-x}/Cr-TiO_{2-x} photoanodes, the X-ray photoelectron spectroscopy (XPS) was conducted. As comparison, the XPS spectra of Cr-SrTiO₃/TiO₂ samples without reduction have also been carried out. The full-scan XPS spectrum of Cr-SrTiO₃/TiO₂ and Cr-SrTiO_{3-x}/Cr-TiO_{2-x} was shown in the Fig. S2. Here, it worth note that no signal of Al element was detected in the reduced sample. Therefore, it could be deduced that the function of Al powder is just reduce the sample and not a dopant.^{2,3} There are two peaks located at 458.1 and 464.0 eV, which can be assigned to Ti 2p_{3/2} and Ti 2p_{1/2}, respectively (Fig. S3A). The binding energies of Ti 2p_{3/2} and Ti 2p_{1/2} in the Cr-SrTiO_{3-x}/Cr-TiO_{2-x} is higher than Cr-SrTiO₃/TiO₂ and the same for the binding energy of the O 1s and Sr 3d (Fig. S3B and D), which may be attributed to the considerable amount of Ti³⁺ states in the Cr-SrTiO_{3-x}/Cr-TiO_{2-x} heterostructures after the Al powder reduced. However, no obviously Ti³⁺ signal was detected, which is absent in our XPS spectrum. Therefore, the XPS study further confirmed that no Ti³⁺ exists on the surface.⁴

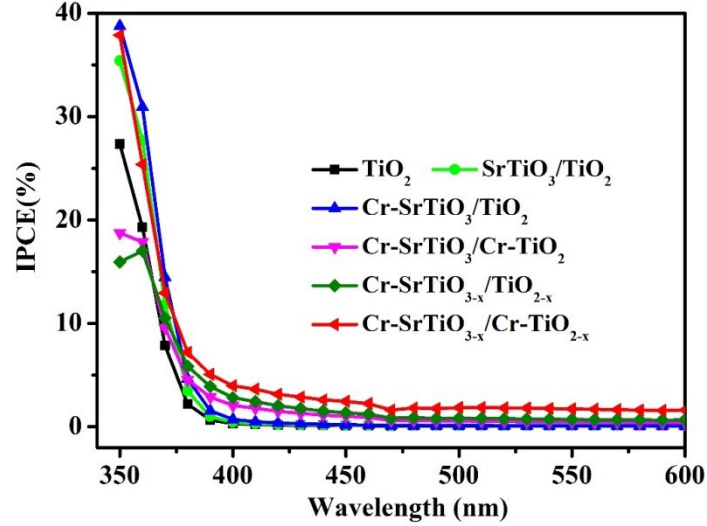


Fig. S4 The IPCE of as-prepared photoanode materials.

Additional discussions

To further understand the relationship between photoelectrochemical response and light absorption, incident photon to current efficiency (IPCE) was measured at an applied of 0.6V (vs SCE) in electrolyte of 1 mol L⁻¹ NaOH solution. In comparison to photocurrent density obtained under white light illumination, incident photon to current conversion efficiency (IPCE) are much better parameters to characterize the photoconversion efficiency of different photoanodes because they are independent from the light sources and filters used in the measurement. The IPCE values were calculated using the following equation as a function of the incident visible light wavelength

$$IPCE(\%) = \frac{1240 \times I(\text{mA}/\text{cm}^2)}{P_{\text{light}}(\text{mW}/\text{cm}^2) \times \lambda(\text{nm})} \times 100$$

Where I is the measured photocurrent density at a specific wavelength, λ is the wavelength of incident light and P_{light} is the measured light power density at that wavelength.

As shown in Fig. S4, the pristine TiO₂ show almost zero photoresponse under the visible light illumination. Compared to the pristine TiO₂, when SrTiO₃/TiO₂ was doped single ion Cr³⁺ or Ti³⁺, the IPCE can obtain obvious ascension. However, for the Cr-SrTiO_{3-x}/Cr-TiO_{2-x} doped with both metal ion Cr³⁺ and Ti³⁺ shows the maximum IPCE up to 4% at 400nm. It indicates that the rational hetero-coupling and metal ion doping could not only effectively narrow their band gaps for extend their photoresponse to visible light region, but also facilitate efficient separation of photoexcited electron-hole pairs. In addition, the IPCE of SrTiO₃/TiO₂ is higher than that of TiO₂ in the range of 380-400nm, indicating the SrTiO₃ response mainly in UV light region due to the

bandgap of SrTiO₃ (3.2 eV).

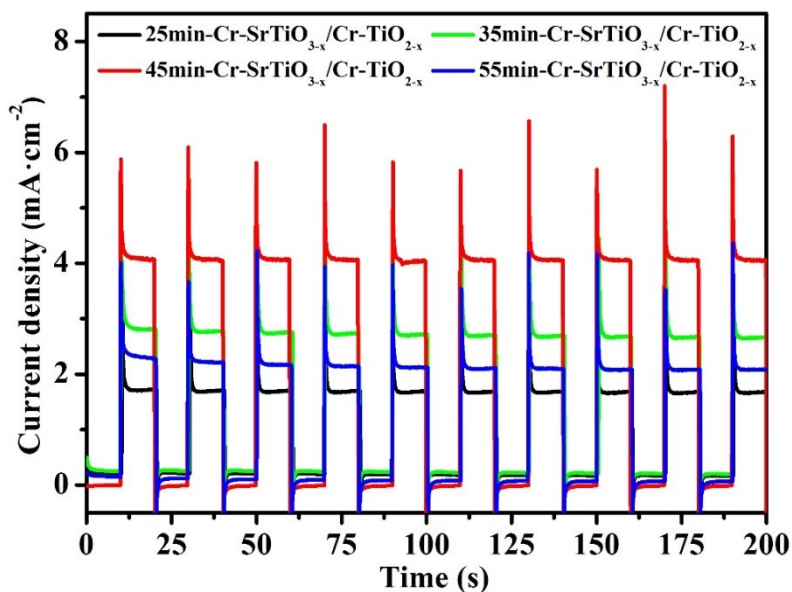


Fig. S5 I-t curves of Cr-SrTiO_{3-x}/Cr-TiO_{2-x} heterostructures after different hydrothermal reaction time.

Additional discussions

To obtain the superior photoelectrochemical performances of Cr-SrTiO_{3-x}/Cr-TiO_{2-x} photoelectrode, the SrTiO₃ nanocubes modified on TiO₂ NTs with different hydrothermal method reaction time was also investigated. As shown in Fig. S5, it can be clearly observed that the photocurrent density of the hydrothermal time for 45 min is much higher than that of other reaction time including 25 min, 35 min and 55 min, which may be due to the suitable amount of SrTiO₃ nanocubes. When the hydrothermal time is 25 min, too little reaction time to form enough SrTiO₃ resulting in lower photocurrent density. Adding the hydrothermal reaction time to 55 min, excess SrTiO₃ nanocubes are grafted on the surface of TiO₂ nanotube arrays, which severely hinder the light absorption of TiO₂ and go against the transport of photoexcited electrons.^{5, 6} It can be concluded that hydrothermal time of 45 min is best reaction conditions.

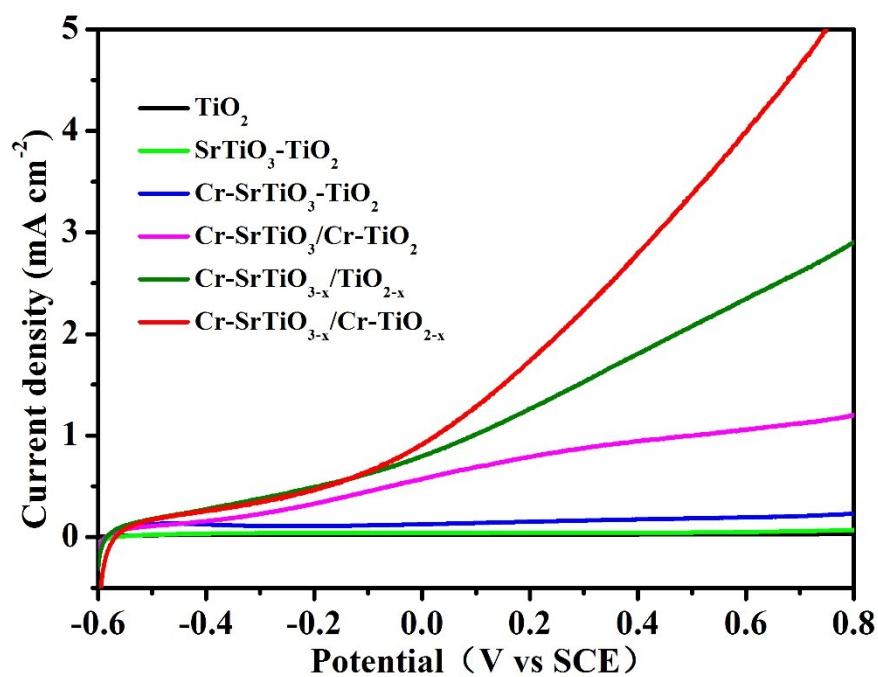


Fig. S6 A) Linear-sweep voltammograms measured in a 1 mol L⁻¹ NaOH solution under visible-light illumination ($\lambda > 420$ nm) of TiO_2 , $\text{SrTiO}_3\text{/TiO}_2$, $\text{Cr-SrTiO}_3\text{/TiO}_2$, $\text{Cr-SrTiO}_3\text{/Cr-TiO}_2$, $\text{Cr-SrTiO}_{3-x}\text{/TiO}_{2-x}$ and $\text{Cr-SrTiO}_{3-x}\text{/Cr-TiO}_{2-x}$.

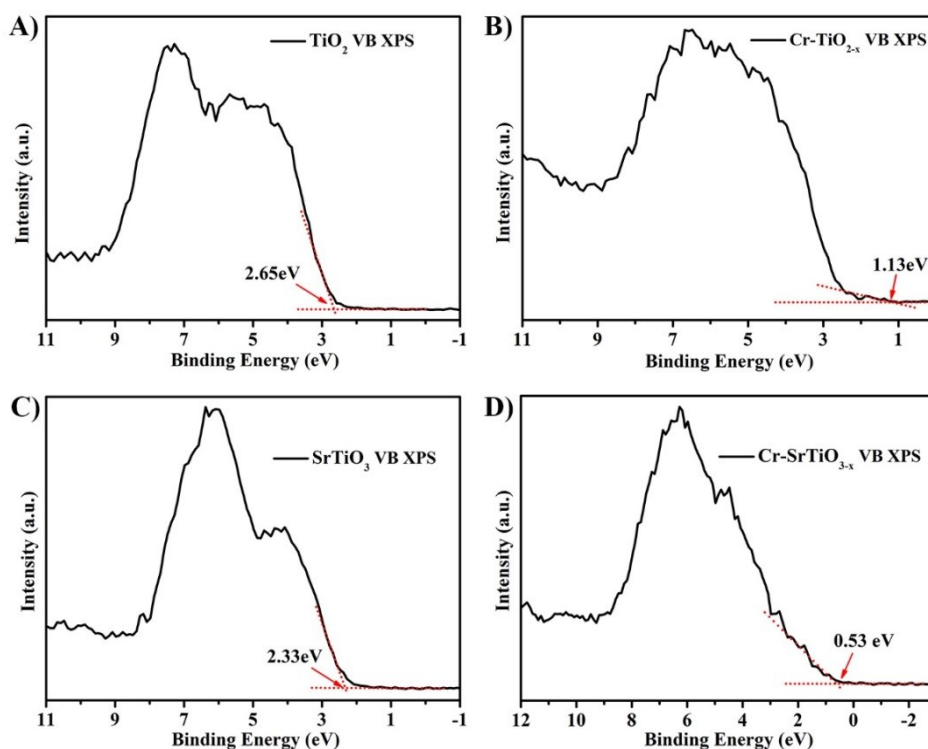


Fig. S7 XPS valence band spectra of A) TiO_2 , B) Cr-TiO_{2-x} , C) SrTiO_3 and D) Cr-SrTiO_{3-x} .

Additional discussions

To reveal the valence band information of Cr-TiO_{2-x} and Cr-SrTiO_{3-x} , the XPS valence band spectra was studied. The valence band maxima are estimated by linear extrapolation of the peaks to the baselines. As shown in Fig. S7, the valence band maximum shifts from 2.65 eV of TiO_2 to 1.13 eV of Cr-TiO_{2-x} . Equally, when SrTiO_3 was doped, the valence band maximum also transform from 2.33eV to 0.53eV. It may be due to that the Cr^{3+} and Ti^{3+} generate some localized states above the valence band edge and result in the bandgap narrowing.⁷

As we all know, the valence band position measured by XPS valence band spectra is relative to the Fermi level. In order to unify the reference, the VB position in vacuum level was calculated. In addition, the work function of TiO_2 and SrTiO_3 is 4.5 eV.^{8,9} According to the equation below:

$$E_{\{\text{vacuum level}\}} = E_{\{\text{Work function}\}} + E_{\{\text{Fermi level}\}} \quad (1);$$

The valence band position of Cr-TiO_{2-x} and Cr-SrTiO_{3-x} relative to the vacuum level are equal to -5.63 eV and -5.03 eV, respectively.

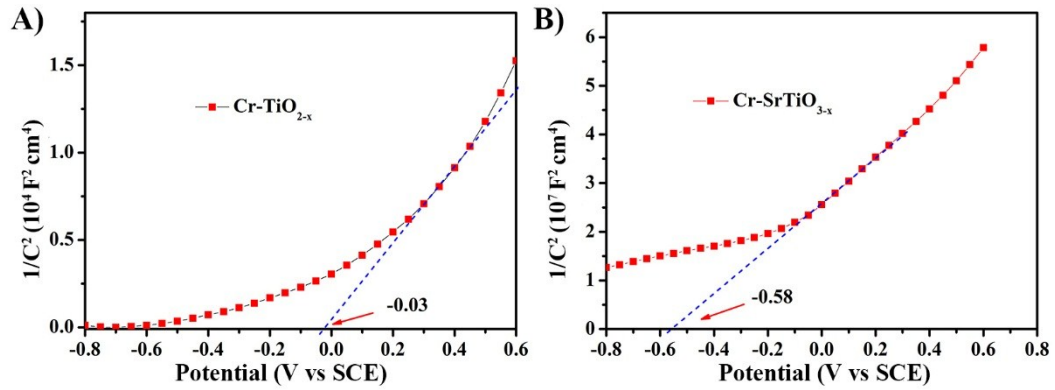


Fig. S8 Mott-Schottky plots for Cr-SrTiO_{3-x} and Cr-TiO_{2-x}.

Additional discussions

Fig. S8 displays the Mott-Schottky plots of $1/C^2$ as a function of the applied potential, from which the positive slopes (i.e., lines) are observed for both Cr-TiO_{2-x} and Cr-SrTiO_{3-x}, suggesting n-type semiconductors. Furthermore, the plots were extrapolated to $1/C^2 = 0$ to estimate the values of E_{FB} (flat band potential), giving -0.03 and -0.58 V for Cr-TiO_{2-x} and Cr-SrTiO_{3-x}, respectively. In addition, for moderately doped n-type semiconductors, there is the semi empirical formula:

$$E_{CB} = E_{FB} - 0.5 (V_{NHE}) \quad (2);$$

Conversion formula between vacuum level and NHE:

$$E_{\text{vacuum level}} = -E_{\text{NHE}} - 4.5 \quad (3);$$

$$E_{\text{NHE}} = E_{\text{SCE}} + 0.24 \quad (4);$$

$$E_{\text{vacuum level}} = -E_{\text{SCE}} - 4.74 \quad (5);$$

According to the above formula, the E_{CB} of Cr-TiO_{2-x} and Cr-SrTiO_{3-x} related to vacuum level is -4.21 eV and -3.42 eV, respectively.

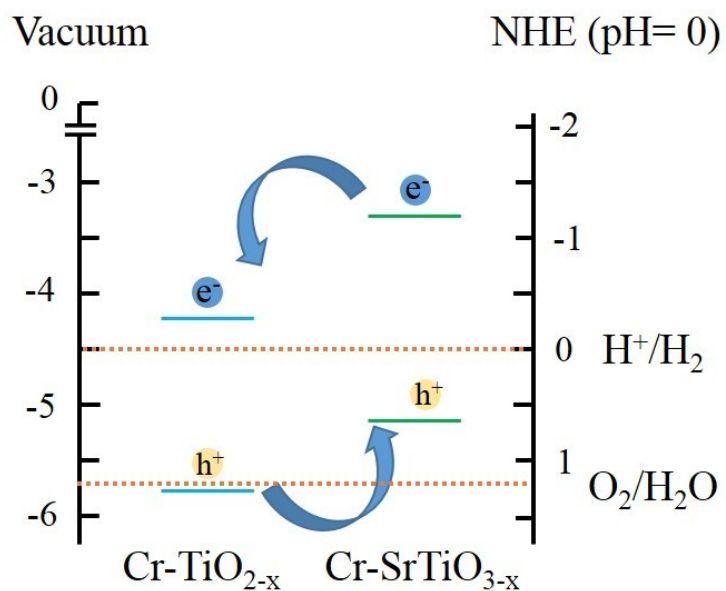


Fig. S9 Energy band position of Cr-TiO_{2-x} and Cr-SrTiO_{3-x}.

Additional discussions

As shown in Fig.S9, the energy band position of Cr-TiO_{2-x} and Cr-SrTiO_{3-x} was signed, according to the measurement result of valence band spectrum of XPS and Mott–Schottky plots (Fig. S7 and S8). Under the visible light irradiation, since the VB edge potentials of Cr-TiO_{2-x} (-4.21 eV) is more negative than Cr-SrTiO_{3-x} (-3.42 eV), the holes of Cr-TiO_{2-x} will transfer to the Cr-SrTiO_{3-x}, due to the action of potential energy. Similarly, the CB edge potentials of Cr-SrTiO_{3-x} (-5.03 eV) is more positive than Cr-TiO_{2-x} (-5.63 eV), the photogenerated electrons of Cr-SrTiO_{3-x} will spontaneous flow to the Cr-TiO_{2-x}.

Notes and references

- 1 J. Zhang, J. H. Bang, C. Tang and P. V. Kamat, *ACS nano*, 2010, **4**, 387-395.
- 2 H. L. Cui, W. Zhao, C. Y. Yang, H. Yin, T. Q. Lin, Y. F. Shan, Y. Xie, H. Gu and F. Q. Huang, *J. Mater. Chem. A*, 2014, **2**, 8612-8616.
- 3 C. Yang, Z. Wang, T. Lin, H. Yin, X. Lu, D. Wan, T. Xu, C. Zheng, J. Lin, F. Huang, X. Xie and M. Jiang, *J. Am. Chem. Soc.*, 2013, **135**, 17831-17838.
- 4 J. Wang, P. Zhang, X. Li, J. Zhu and H. Li, *Appl. Catal., B*, 2013, **134-135**, 198-204.
- 5 M. Shang, H. Hu, G. Lu and Y. Bi, *J. Mater. Chem. A*, 2016, **4**, 5849-5853.
- 6 Z. Jiao, Y. Zhang, T. Chen, Q. Dong, G. Lu and Y. Bi, *Chem. Eur. J.*, 2014, **20**, 2654-2662.
- 7 X. Chen, L. Liu, P. Y. Yu and S. S. Mao, *Science*, 2011, **331**, 746-750.
- 8 G. Liu, F. Li, D. W. Wang, D. M. Tang, C. Liu, X. Ma, G. Q. Lu, and H. M. Cheng, *Nanotechnology*, 2008, **19**, 025606.
- 9 H. Zhang, D. Zhang, X. Lu, C. Liu, G. Zhou, X. Ma, L. Wang, P. Jiang, Q. Xue, X. Bao, *Nat. commun.*, 2017, **8**, 214-220.